J Bioenerg Biomembr (2011) 43:311–322
DOI 10.1007/s10863-011-9354-7

Action potentials in primary osteoblasts and in the MG-63 osteoblast-like cell line

Maria Pangalos · Willem Bintig · Barbara Schlingmann · Frank Feyerabend · Frank Witte · Daniela Begandt · Alexander Heisterkamp · Anaclet Ngezahayo

Received: 2 January 2011 / Accepted: 3 April 2011 / Published online: 27 April 2011

Abstract Whole-cell patch-clamp analysis revealed a resting membrane potential of −60 mV in primary osteoblasts and in the MG-63 osteoblast-like cells. Depolarization-induced action potentials were characterized by duration of 60 ms, a minimal peak-to-peak distance of 180 ms, a threshold value of −20 mV and a repolarization between the spikes to −45 mV. Expressed channels were characterized by application of voltage pulses between −150 mV and 90 mV in 10 mV steps, from a holding potential of −40 mV. Voltages below −60 mV induced an inward current. Depolarizing voltages above −30 mV evoked two currents: (a) a fast activated and inactivated inward current at voltages between −30 and 30 mV, and (b) a delayed-activated outward current that was induced by voltages above −30 mV. Electrophysiological and pharmacological parameters indicated that hyperpolarization activated strongly rectifying K^+ (K_{ir}) channels, whereas depolarization activated tetrodotoxin sensitive voltage gated Na^+ (Na_v) channels as well as delayed, slowly activated, non-inactivating, and tetraethylammonium sensitive voltage gated K^+ (K_v) channels. In addition, RT-PCR showed expression of $Na_v1.3$, $Na_v1.4$, $Na_v1.5$, $Na_v1.6$, $Na_v1.7$, and $K_{ir}2.1$, $K_{ir}2.3$, and $K_{ir}2.4$ as well as $K_v2.1$. We conclude that osteoblasts express channels that allow firing of action potentials.

Keywords Osteoblasts · MG-63 cells · Action potential · K_{ir} · K_v · Na_v · RT-PCR

M. Pangalos · W. Bintig · B. Schlingmann · D. Begandt · A. Ngezahayo
Institute of Biophysics, Leibniz University of Hannover, Herrenhäuserstr. 2, 30419 Hannover, Germany

B. Schlingmann · A. Ngezahayo (✉)
Center for Systemic Neuroscience (ZSN), Hannover, Germany
e-mail: ngezahayo@biophysik.uni-hannover.de

F. Feyerabend
Department for Structural Research on Macromolecules, Helmholtz-Zentrum Geesthacht, Institute of Materials Research, Max-Planck-Str. 1, 21502 Geesthacht, Germany

A. Heisterkamp
Laser Zentrum Hannover e.V, Hollerithallee 8, 30419 Hannover, Germany

F. Witte
Implant-Immunology, CrossBIT - Center for Biocompatibility and Implant-Immunology, Hannover Medical School, Feodor-Lynen-Str. 31, 30625 Hannover, Germany

Introduction

Repetitive action potentials, in response to a long lasting membrane depolarization, are a characteristic of excitable cells, such as neurons, muscle cells or endocrine cells. The generation of action potentials is possible when cells express special types of voltage-gated channels (Bezanilla 2007; Clay 2005; Hodgkin and Huxley 1952). These channels are closed when the membrane potential is maintained near the resting membrane potential and they open sequentially in response to membrane depolarization above a defined threshold value. Voltage-gated Na^+ (Na_v) channels are the first channels that are opened by depolarization. These channels allow an inward flow of Na^+, which in turn, produces further depolarization of the membrane. This effect causes more Na_v channels to open and produces an even greater electrical current. The process

proceeds explosively, which results in a large increase in the membrane potential toward the equilibrium potential for Na^+ (E_{Na^+}), before the Na^+ channels rapidly inactivate. Parallel to the Na_v inactivation, the delayed voltage-activated K^+ (K_v) channels open, which gives rise to an outward K^+ current. The increase in the membrane permeability to K^+ repolarises the membrane toward the equilibrium potential for K^+ (E_{K^+}). After an action potential has occurred, there is a transient negative shift of the membrane potential, referred to as after hyperpolarization. The after hyperpolarization activates inwardly rectifying K^+ (K_{ir}) channels. The K_{ir} channels reset the membrane potential to the resting value by allowing a flux of K^+ ions through the membrane. All of the different channels have specific activation and pharmacological properties, which allow their identification.

The Na_v channels, which are responsible for the rising phase of the action potential, are formed at the molecular level by the association of a set of pore-forming α and subsidiary β (β_1, β_2 or β_3) subunits (Catterall et al. 2003; Hanck and Fozzard 2007). The pore-forming α subunit is a product of a gene family with nine members from the Na_V1 gene family. The channels are denominated as $Na_V1.x$, where x is a number and denotes the specific channel isoform and corresponds approximately to the order that each gene was identified. Accordingly, the channels are named $Na_V1.1$–1.9. The pore-forming subunits are formed by four large regions, each comprising six transmembrane (TM) domains and a P-loop between the fifth and the sixth TM helices. The association of the four P-loops form a pore through the membrane.

At the pharmacological level, the Na_V channels are characterized by their sensitivity to tetrodotoxin (TTX) and saxitoxin (STX). The channels are classified as either TTX sensitive or TTX resistant, depending on the TTX concentration that is necessary to inhibit the Na_V channels (Bosmans and Tytgat 2007; Koopmann et al. 2006; Lei et al. 2004; Narahashi 2008). The TTX sensitive Na_v channels are inhibited by TTX concentrations of 10–100 nM, while the TTX resistant channels are blocked by TTX concentrations in the μM ranges (Lei et al. 2004). The TTX sensitivity is related to the presence of an aromatic amino acid residue (Y or F) at position 401 in the P-loop of the first large region (Fozzard and Lipkind 2010; Lee and Ruben 2008; Lipkind and Fozzard 1994; Penzotti et al. 2001). Genetic and pharmacological studies have shown that $Na_V1.1$–1.4, 1.6, and 1.7 are TTX sensitive, while $Na_V1.5$, 1.8, and 1.9 are TTX resistant (Goldin 2002; Koopmann et al. 2006; Lei et al. 2004; Narahashi 2008).

The K_V channels are responsible for the repolarization of the membrane. They are formed by association of four pore-forming α and four β auxiliary subunits. The pore-forming α subunits of the K_V channels have six transmembrane domains. They are produced by the K_v channel gene subfamily, which comprises four members, named *shaker*, *shab*, *shaw*, and *shal*, or K_v1, K_v2, K_v3, and K_v4, respectively. Each subfamily has characteristic activation and inactivation kinetic, as well as pharmacological sensitivity (Heitzmann and Warth 2008; Nerbonne 2000; Song 2002). Despite contradictory observations, it is generally accepted that the members of the K_v1 channels have a fast activation, a slow inactivation and are sensitive to 4-aminopyridine (4-AP). The K_v3 channels activate very quickly but inactivate slowly and are sensitive to tetraethylammonium (TEA). The K_v4 channels are fast activated and inactivated, and are sensitive to 4-AP. The K_v2 channels activate slowly and do not inactivate, and are inhibited by high TEA concentrations (Nerbonne 2000). The fast activating channels, K_v1, K_v3, and K_v4, are responsible for brief action potentials (Korn and Trapani 2007) because they repolarize the membrane very quickly.

The K_{ir} channels belong to the family of two transmembrane domain (2 TM) K^+ channels with a pore forming region between the transmembrane domains (Heitzmann and Warth 2008). Despite originating from 16 different genes, all K_{ir} channels share common properties. Each K_{ir} channel is formed by four α subunits assembled as homomer or heteromer. In all cases, the inward current increases with increasing external K^+ concentration ($[K^+]_o$), which indicates high specificity for K^+. The most defining feature shared by all of the K_{ir} channels is the reversible blockage by externally applied Ba^{2+} (Olsen and Sontheimer 2008). As the name implies, the K_{ir} channels preferentially conduct an inward current, although some subunits allow for outward currents. It is noteworthy that K_{ir} channels, while rectifying, are not voltage dependent. The apparent voltage sensitivity of these channels is related to a blockage of the channels by intracellular Mg^{2+} or polyamine ions, which are pushed into the channel pore by voltages above the E_{K^+} (Oliver et al. 2000; Panama and Lopatin 2006; Ruppersberg 2000). This effect increases with membrane potentials that are more positive than E_{K^+}, resulting in a reduction of outward K^+ currents through the K_{ir} channels. While all K_{ir} channels rectify and pass K^+ ions into the cell more readily than they allow for K^+ efflux, the degree of rectification varies between the channel subtypes. The $K_{ir}1$, $K_{ir}4$, $K_{ir}5$, and $K_{ir}7$ subfamilies are weak inward rectifiers that permit considerable outward K^+ currents, while the $K_{ir}2$ and $K_{ir}3$ subfamilies rectify strongly, permitting little K^+ efflux (Bichet et al. 2003; de Boer et al. 2010; Hibino et al. 2010; Ruppersberg 2000). Moreover, the different K_{ir} channels have specific pharmacology. The $K_{ir}1$ and $K_{ir}4$ channels are sensitive to pH. Internal acidification to pH values below 6.5 closes the channels (Dahlmann et al. 2004; Pearson et al. 1999). The $K_{ir}3$ channels are activated by G protein-coupled receptors (Hibino et al. 2010). The

$K_{ir}6$ proteins form the K_{ATP} channels that are closed by internal ATP (Flagg et al. 2010; Hibino et al. 2010). A feature that is common to all vertebrate K_{ir} currents is a slow time-dependent inactivation, which increases with the hyperpolarization and creates the negative bend in the current/voltage (*I(V)*) plot. While this could be interpreted as voltage-dependent gating, it actually reflects a voltage-dependent block of these channels by external Na^+ ions (Lee et al. 2007).

In this report, we show that primary osteoblasts and the osteoblast-like MG-63 cell line express sequentially activated Na_v, K_v and K_{ir} channels, which allow the cells to generate repetitive action potentials in response to a long lasting depolarization. Herein, we discuss a potential role for the action potential in osteoblasts in processes such as differentiation, bone formation, and pathology.

Materials and methods

Chemicals

If not otherwise stated, all chemicals and cell culture media were obtained from Sigma-Aldrich (Taufkirchen, Germany).

Cell culture

Primary human osteoblasts were cultured from bone chips obtained from patients undergoing total hip arthroplasty, following the protocol set by Gallagher (2003). The isolation protocol was approved by the local ethics committee of the Institute of Materials Research in Geesthacht, Germany. Briefly, cancellous bone was cut into 5-mm pieces. After removal of bone marrow, the bone chips were cultured in Dulbecco's modified eagle medium (DMEM) supplemented with 10% fetal bovine serum (PAA Laboratories GmbH, Linz, Austria), 100 U/ml penicillin, and 100 μg/ml streptomycin. The culture was maintained for approximately 10 days without medium change. Thereafter, the medium was changed every 3 days and cells were passaged after reaching 70–80% confluency.

The human osteosarcoma cell line, MG-63, was obtained from the European collection of cell cultures (ECACC, Salisbury, UK). They were cultured in DMEM supplemented with 10% foetal bovine serum, 100 U/ml penicillin, and 100 μg/ml streptomycin. The cultures were maintained at 37 °C in a humidified atmosphere containing 5% CO_2 and 95% air. The culture medium was replaced every 2 to 3 days.

For patch-clamp experiments, cover slips (Ø 10 mm) were placed into dishes containing 4 ml of DMEM culture medium. The cells were seeded at a density of 1×10^5 cells/dish. The cells were used 1 to 3 days after seeding. For the primary cells, the cover slips were coated with collagen. The primary cells were cultured and used for up to five passages. For the MG-63 osteoblast-like cells, the cells were used up to passage 30.

For the RT-PCR experiments, the cells were cultured for 2 to 5 days and harvested when they were at least 80% confluent.

Functional identification of the expressed channels

The whole-cell patch-clamp technique was used to measure the different currents of the cells. All experiments were performed at room temperature. A cover slip with the cells was placed in a perfusion chamber containing 0.5 ml of a bath solution composed of (in mM): 145 NaCl, 5 KCl, 2 $CaCl_2$, 1 $MgCl_2$, 5 glucose, and 10 HEPES, (pH 7.4, 295 mosmol/l). The perfusion chamber was mounted onto an inverted microscope (Zeiss, Oberkochen, Germany). The cells were washed with 10 ml of bath solution at 1 ml/s. To visualise the cells, a CCD camera (Sony, Japan) and a video monitor was used. To navigate the patch-clamp capillaries onto the cells, a micromanipulator (Merzhäuzer, Wetzlar-Steindorf, Germany) was used. The patch-clamp capillaries were filled with a pipette solution that contained (in mM): 145 K-gluconat, 5 KCl, 0.5 Na_2ATP, 2.5 MgATP, 0.5 $CaCl_2$, 1 EGTA, 1 glucose, and 10 HEPES (pH 7.4, 295 mosmol/l). To induce action potentials, depolarizing currents were injected into the cells under a current-clamp modus with the patch-clamp amplifier EPC-7 (List Medical, Darmstadt, Germany) connected to a computer through an ITC-16 interface (Instrutech, Port Washington, USA). The currents were measured in voltage-clamp modus. From a constant holding voltage of −40 mV, test voltage pulses were applied from −150 mV to 90 mV for 1 s in 10 mV steps. The evoked currents were filtered at 3 kHz and sampled at 10 kHz. Pulse protocols, data acquisition, and analysis were performed using Pulse/PulseFit (HEKA, Lambrecht/Pfalz, Germany), Excel 2004 (Microsoft, Redmond, USA) and OriginPro 7.5 (Microcal Software, Inc., Northampton, USA).

Data analysis

The voltage-dependent channels were analyzed between −150 mV and −60 mV with the amplitudes of the instantaneous current ($I_{(inst)}$) at the beginning of the voltage pulses measured and plotted against the corresponding voltage in an *I(V)* plot. To describe the voltage dependence of the conductance of the channels, the macroscopic conductance (G) was calculated from the instantaneous current amplitudes, normalized to the maximal conductance (G_{max}). The corresponding values were plotted against the voltage in a $G(V)/G_{max}$ diagram. To estimate the activation

parameters of the channels, the data points were fit with a simple Boltzmann distribution as given by the equation: $G/G_{\max} = 1/\left(1 + e^{(U-U_{1/2})\cdot\frac{zF}{RT}}\right)$, where R, T, F have their usual meanings, $U_{1/2}$ represents the half-activation voltage at the point where 50% of the maximal conductance was reached, and z represents the number of apparent gating charges. Additionally, the steady state currents ($I_{(ss)}$) at the end of the voltage pulses were measured and plotted against the corresponding voltage in an $I_{ss}(V)$ plot. To account for the inactivation of the channels, the current-time relaxation between the instantaneous amplitude $I_{(inst)}$ and the steady state amplitude $I_{(ss)}$ was fit to the following single exponential function: $I_{(t)} = (I_{(inst)} - I_{(ss)}).e^{-\frac{t}{\tau_i}} + I_{(ss)}$, where τ_i gives the voltage-dependent inactivation time.

Between −30 mV and 30 mV, the maximum amplitude of the voltage-activated inward current was measured and plotted against the corresponding voltage in an *I(V)* plot. To describe the voltage dependence of the conductance of the channels, the macroscopic conductance (G) was calculated from the maximal amplitudes of the currents and plotted in a $G(V)/G_{max}$ diagram, and the activation parameters of the channels were obtained by fitting the data points with a simple Boltzmann distribution as described above.

Between −30 mV and 90 mV, the activated, delayed-activated outward currents were analysed in two steps. First, the amplitudes of the steady state currents ($I_{(ss)}$) at the end of the voltage pulse were measured and plotted against the corresponding voltage in an *I(V)* plot. As described above, the macroscopic conductance (G) was calculated from the steady state current amplitudes, a $G(V)/G_{max}$ diagram was produced, and the data points were fit to a simple Boltzmann distribution to estimate the activation parameters of the channels. Second, the activation kinetics were estimated for each voltage pulse by fitting the time dependent increase of the current using the following simple exponential function: $I_{(t)} = (I_{(inst)} - I_{(ss)}).e^{-\frac{t}{\tau a}} + I_{(ss)}$, where $I_{(inst)}$ and $I_{(ss)}$ are the instantaneous and the steady state current amplitudes, respectively, and τ_a gives the voltage dependent activation time.

Channel screening by RT-PCR

Total RNA from MG-63 cells (about 2 million cells) was extracted using the Qiagen RNeasy Mini Kit (Qiagen, Hilden, Germany). Genomic DNA was removed by digestion with RNase-free DNase (Fermentas, St. Leon-Rot, Germany) for 60 min at 37 °C. First strand cDNA synthesis of the total RNA using the M-MLV reverse transcriptase (Invitrogen GmbH, Karlsruhe, Germany) was performed according to the manufacturer's protocol with a hexamer primer. cDNA fragments of the various K_{ir}, K_v, and Na_v channel subtypes were amplified using a set of designed sense and antisense primers (Primer-BLAST, http://www.ncbi.nlm.nih.gov), as shown in Table 1. PCR experiments were run on a 96 Universal Gradient PeqStar Thermocycler (PeqLab, Erlangen, Germany) in a final volume of 25 μl containing

Table 1 List of the primers used for the RT-PCR

Gene name	Accession no.	Forward primer (5′ -> 3′)	Reverse primer (5′ -> 3′)	Product size (bp)
$Na_v1.1$	NM_001165963	TGTTTCACTGAAGGCTGTGTACAA	GCCAACACCAGGCATTGGTG	322
$Na_v1.2$	NM_021007	TCACGAAATGTAGAATTACAACCCA	TCAAAGACTTGTTTGGTTACAAAATCA	302
$Na_v1.3$	NM_006922	TTCAGTGTCATTGTGATGGCA	TTGGTTTCAAAAGCAGAATCGC	287
$Na_v1.4$	NM_000334	GGAGTCACTGGCAGCCATAG	CATGCTGAACAGCGCATGGA	340
Na_v 1.5	NM_198056	CAAGTGAATTCGAGGAGATGCT	CCGATGATCTTGATGAGTGTGT	274
$Na_v1.6$	NM_014191	CTAGGCAAGTCTTGGTGGATC	CAGCCACAATGAGGAAGTCC	283
$Na_v1.7$	NM_002977	GGCTGTCGGCTTTCCAATT	GGCAACATTGCCATCTTTTCA	276
$Na_v1.8$	NM 006514	TCCCCATTGGATCCCTCGAA	AAATAAACTGAACCACGAGTGGA	398
$Na_v1.9$	NM_014139	GCAGGCTGTTTTATTCCCGC	ACATGCTGAACAATGAATGGACTG	472
$K_{ir}2.1$	NM_000891	TCGCTTTTTACAAACCACTGGA	TTCTGCTTTGGAAAACAGTCTGA	277
$K_{ir}2.2$	NM_021012	ATCCGCTTTGCAGAGAAGAC	GCGGCTCCTCTTGAGTTC	300
$K_{ir}2.3$	NM_152868	GGTGGGGGTTTCAAAGACTG	ACAGTCATGCAAAAGAAACGC	286
$K_v2.1$	NM_013348	GCTGGTCTTCAGCGAGAAC	TAGCTCATACAGAGGACTGGC	271
$K_v2.1$	NM_004975	ACCTACTGGAGAAGCCCAATT	TAGTATGGCAGAATGGCCAAC	292
$K_v2.2$	NM_004770	ATGAACGAAGAACTGAGGCG	TGCTAATTGGCGGTTGTCATT	261
$K_v3.1$	NM_004976	GAGATGACCAAGCGCCTG	ATGTAGGTAAGGAAGGCCTCC.	296
$K_v3.2$	NM_139136	ATCCGCAGATCACAGAATGAAG	GTTCTCGATCTTGCCCATCTC	272

45 ng of first strand cDNA as the template. The amplification was performed in 44 cycles (15 s at 94 °C, 15 s at 53±2 °C, and 15 s at 72 °C). The PCR products were separated on 1.5% agarose gels and stained with GelRed (Biotium, Hayward, CA, USA).

Results

The firing of repetitive action potentials (Fig. 1) were induced in the primary isolated osteoblasts and in the osteoblast-like MG-63 cell line by injecting a depolarizing current under the current-clamp modus of the whole-cell patch-clamp configuration. The action potentials were characterized by a long duration (60 ms), a high threshold (−20 mV), a non-complete repolarization between the spikes, and a low frequency (a maximum of 5–6 Hz). The generation of repetitive action potentials in cells such as neurons or muscle cells is related to the concomitant expression and sequential activation of voltage-gated sodium (Na_v) and potassium (K_v) channels (Hodgkin and Huxley 1952). Additionally, the inwardly rectifying potassium channels (K_{ir}) can participate in the generation of action potentials by controlling the resting membrane potential. Because we observed that the osteoblasts were able to generate action potentials, we analysed the voltage-dependent activation of the currents within the cells. In the primary osteoblasts, as well as in the MG-63 cells, we found a resting membrane potential of approximately −60 mV. To evaluate the ion channels expressed in the membranes of the cells, the cells were maintained at a holding potential of −40 mV and voltage pulses from −150 mV to 90 mV were applied for 1 s in 10 mV steps. Three distinct currents could be observed (Fig. 2): (a) an inward current activated by hyperpolarising voltages below −60 mV, (b) an inward current activated by depolarizing voltages between −30 mV and 30 mV, and (c) a delayed-activated outward current evoked by depolarizing voltages above −30 mV. Because these currents were observed in primary osteoblasts and in the osteoblast-like MG-63 cell line, the MG-63 cells were used for the further functional characterization of the currents. In following, the electrical and pharmacological behaviour of these currents will be described.

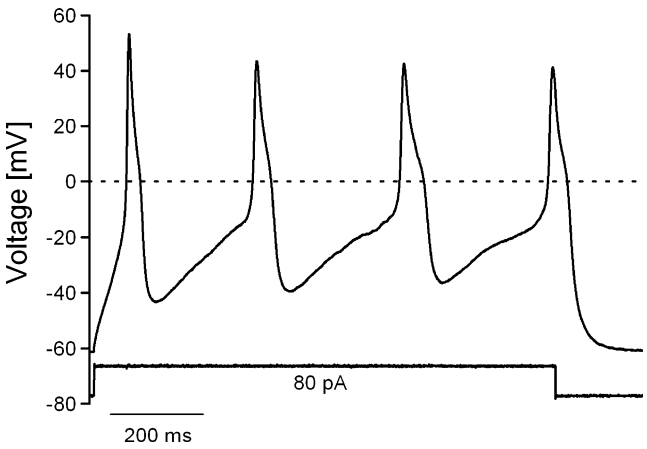

Fig. 1 Depolarization induced action potentials. The injection of currents between 50 and 100 pA generated action potentials in the cells. The frequency increased with the intensity of the depolarizing current to a maximum of six spikes during the depolarization period (1 s)

The hyperpolarization activated inward current

The hyperpolarization-activated inward current was instantaneously activated between −60 mV and −150 mV in a voltage dependent manner. The instantaneous current was followed by a steady-state current (Fig. 2a). The steady-state current increased with hyperpolarization until −100 mV (Fig. 2b). At larger hyperpolarizing voltages, an inactivation of the current was observed (Fig. 2a and b). The hyperpolarization-activated inward current, which was observed at very low Cl^- concentrations in the internal solution, presented the following pharmacology: it was not significantly affected by the Cl^- channel inhibitor, 4,4′-diisothiocyano-2,2′-stilbene disulphonic acid (DIDS), it was inhibited by Ba^{2+} (Fig. 3a), and it was enhanced by an increased $[K]_o$. In addition, the increase in $[K]_o$ suppressed the inactivation of the channel (Fig. 3b). The reverse potential of the current was estimated to be −70 mV and −10 mV at 5 mM and 55 mM of $[K^+]_o$, respectively (Fig. 3b). To determine the voltage-dependent characteristics of the hyperpolarization-dependent currents, we analysed the voltage-dependent activation of the instantaneous currents and the voltage-dependent kinetics of the current relaxation from the instantaneous current to the steady-state amplitudes. For the instantaneous current, macroscopic conductance-voltage ($G(V)$) curves were determined (Fig. 3c). The $G(V)/G_{max}$ diagrams show that the channels opened at hyperpolarizing voltages. The half-maximal voltage of activation ($U_{1/2}$) of −73 mV and the apparent equivalent gating charge (z) of 2.3 were derived by fitting the $G(V)/G_{max}$ curve with a simple Boltzmann function (Fig. 3c). The kinetic of inactivation was voltage dependent. At −100 mV, the inactivation was very slow and the steady-state current could not be achieved during the duration of the pulse (1 s). The inactivation was very rapid at voltages below −120 mV and the steady-state current, representing 10% of the instantaneous current, was achieved within 400 ms (Fig. 2). The relaxation of the inactivated current could be fit by an exponential function, as described in the Materials and Methods (Fig. 3e insert). We found that the inactivation time decreased with hyperpolarization, from 330 ms at −100 mV to 163 ms at hyperpolarizing voltages below −120 mV (Fig. 3d).

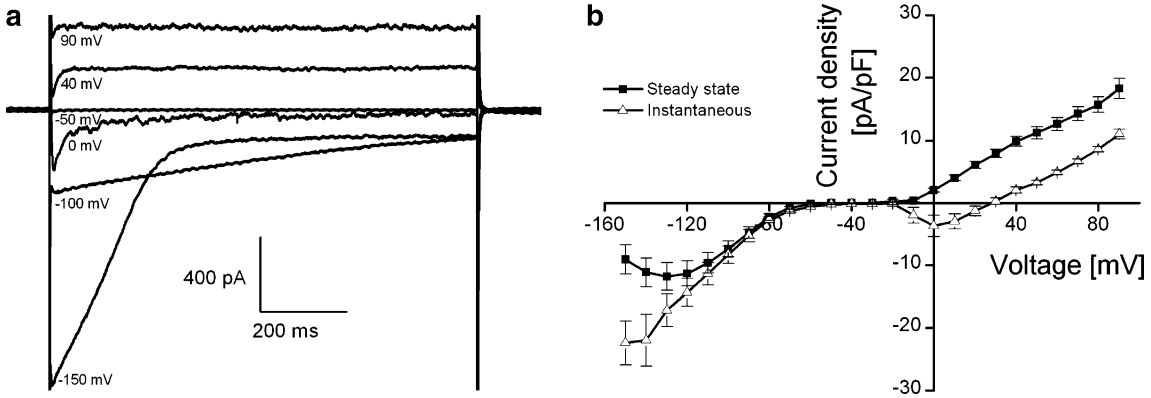

Fig. 2 The current elicited by different voltage pulses. **a** Original traces of the currents evoked by voltage pulses as indicated. Hyperpolarizing voltages between −150 mM and −60 mV induced inward currents. **b** The I(V) diagram of the observed currents. The current voltage relationship (I(V)) of the instantaneous current amplitude and the steady state current amplitude were measured in the first and in the last 10 ms of the voltage pulses. The results are given as an average, and the error bars represent the SEM for eight experiments. In addition, similar currents could be measured in the cultivated primary osteoblasts

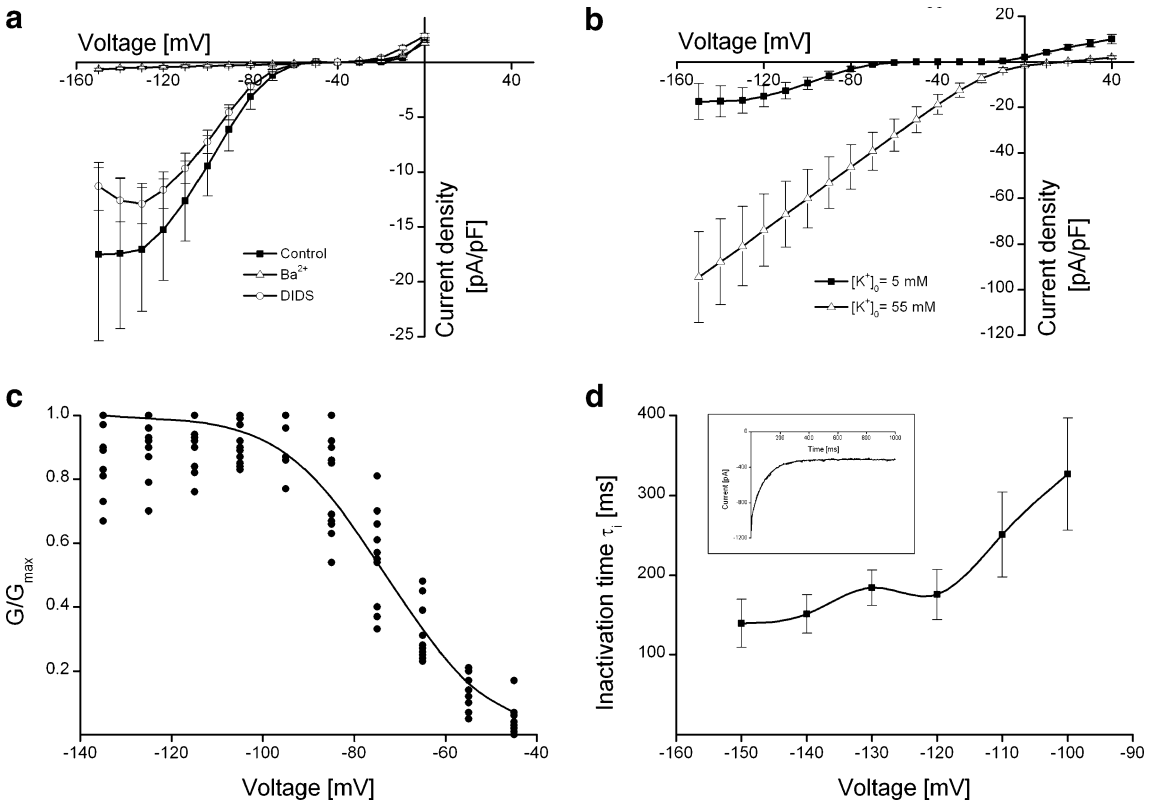

Fig. 3 Pharmacological and electrical characterizations of the hyperpolarization-activated currents. **a** A voltage/current density plot is shown. With respect to the control conditions, the diagram shows that the current was significantly reduced by DIDS and was completely inhibited by Ba^{2+}. The results are averages of 20 (control), nine (Ba^{2+}) and eight (DIDS) cells, the error bars represent the SEM. **b** The current density was potentiated by $[K^+]_o$ increase. The results of each curve are an average of five cells, and the error bars represent the SEM. **c** The voltage-dependent membrane conductance $G(V)/G_{max}$. The solid line represents a fit of the data points with a simple Boltzmann distribution. This allowed us to estimate a half-activation voltage of −73 mV and an apparent gating charge of 2.3. Each point represents an independent experiment ($n=10$). **d** The voltage-inactivation kinetics of the hyperpolarization induced currents. The current relaxation observed at each voltage pulse was fitted with a simple exponential function (insert). The voltage-dependent inactivation time, τ_i, decreased with increasing hyperpolarization. From a maximal value of 330 ms at −100 mV, τ_i reached the minimal value of 164 ms for voltages below −120 mV. The results are given as an average, and the error bars represent the SEM for 29 cells

The depolarization-activated inward current

In 70% of the cells, depolarization of the membrane to voltages above −30 mV induced an inward current (Figs. 1a and 4) with the following characteristics: (a) the maximal amplitude of the current was achieved at 10 mV, (b) the activation and the inactivation of the currents were very fast, and (c) the current was abolished by depolarizations above 30 mV (Fig. 4a). In addition, the depolarization-activated inward current showed a sensitivity to the internal Na^+ concentration ($[Na^+]_i$). At 10 mM internal Na^+, the inward current was continuously reduced to achieve a complete run down within 5–10 min after establishment of the whole-cell configuration (results not shown). The run down was avoided at $[Na^+]_i$ of 1 mM. Additionally, the depolarization-activated inward current was reversibly inhibited by 50 nM TTX (Fig. 4b).

To determine the voltage-dependent characteristics of the depolarization-activated inward current, relative macroscopic conductance-voltage ($G(V)/G_{max}$) curves were determined (Fig. 4c). The $G(V)/G_{max}$ curves show that the currents were induced at voltages above −30 mV. The conductance increased with increasing depolarization to achieve a maximum at a depolarization between 0 and 10 mV. The half-maximal activation voltage ($U_{1/2}$) of −9 mV and the equivalent gating charge (z) of 4.2 were derived by fitting the $G(V)/G_{max}$ curve with a simple Boltzmann distribution.

The depolarization-activated outward current

The delayed-activated outward current was observed in all cells when depolarizing voltages above −30 mV were applied. The current showed a slow activation followed by a steady-state current, $I_{(ss)}$, which increased with increasing voltages (Fig. 2). The depolarization-activated outward current presented the following pharmacology: (a) the Cl^- channel inhibitor DIDS reduced the current by 20–30%, and (b) TEA, the inhibitor of the voltage-dependent K^+ channels, reduced the current by 70–80% (Fig. 5a). To determine the voltage-dependent characteristics of the hyperpolarization-dependent currents, we analyzed the

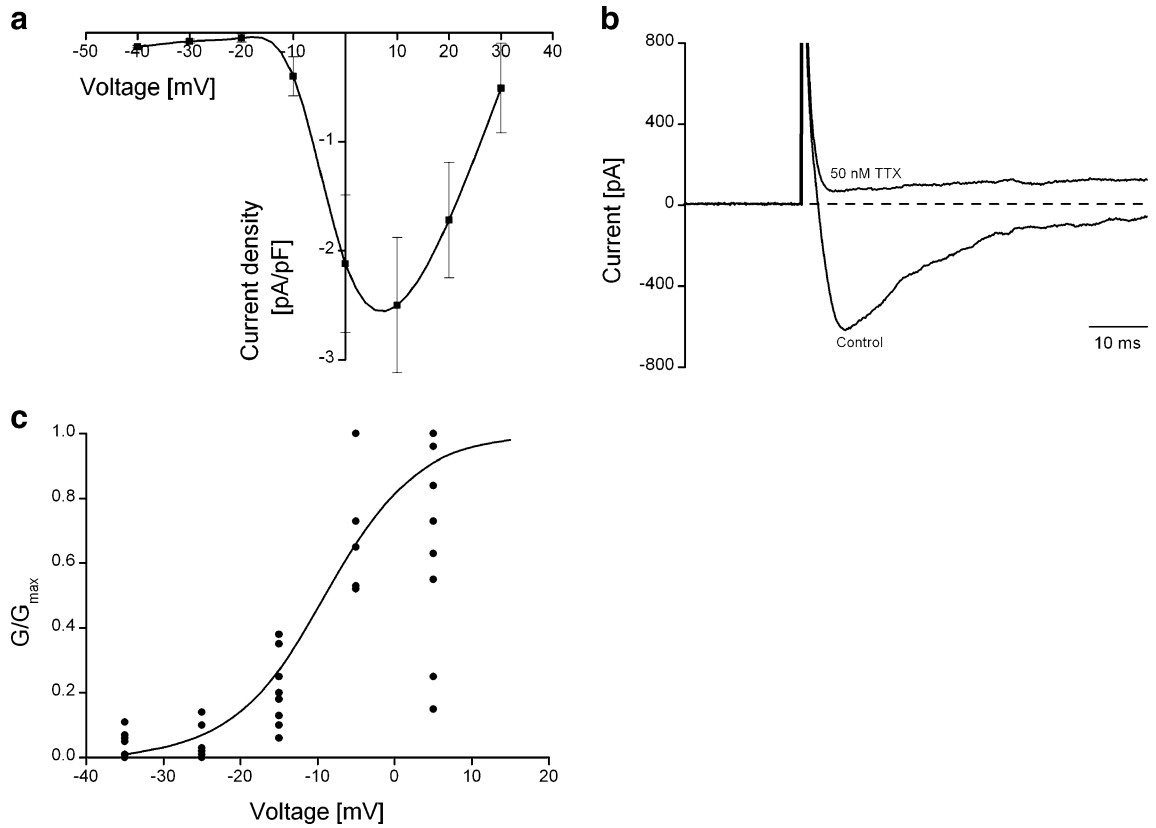

Fig. 4 The depolarization-activated inward current. **a** The diagram shows the maximal current density evoked by the different voltage pulses. These currents were observed in 73% of the cells (16 out of 22). The resulting curve is an average of 16 cells, the error bars represent the SEM. **b** The current could be suppressed by 50 nM TTX. The TTX inhibition was reversible (not shown). **c** The voltage-dependent membrane conductance $G(V)/G_{max}$. The solid line represents a fit of the data points with a simple Boltzmann function. A half-activation voltage, $U_{1/2}$, of −9 mV and an apparent gating charge, z, of 4.2 were estimated (n=9)

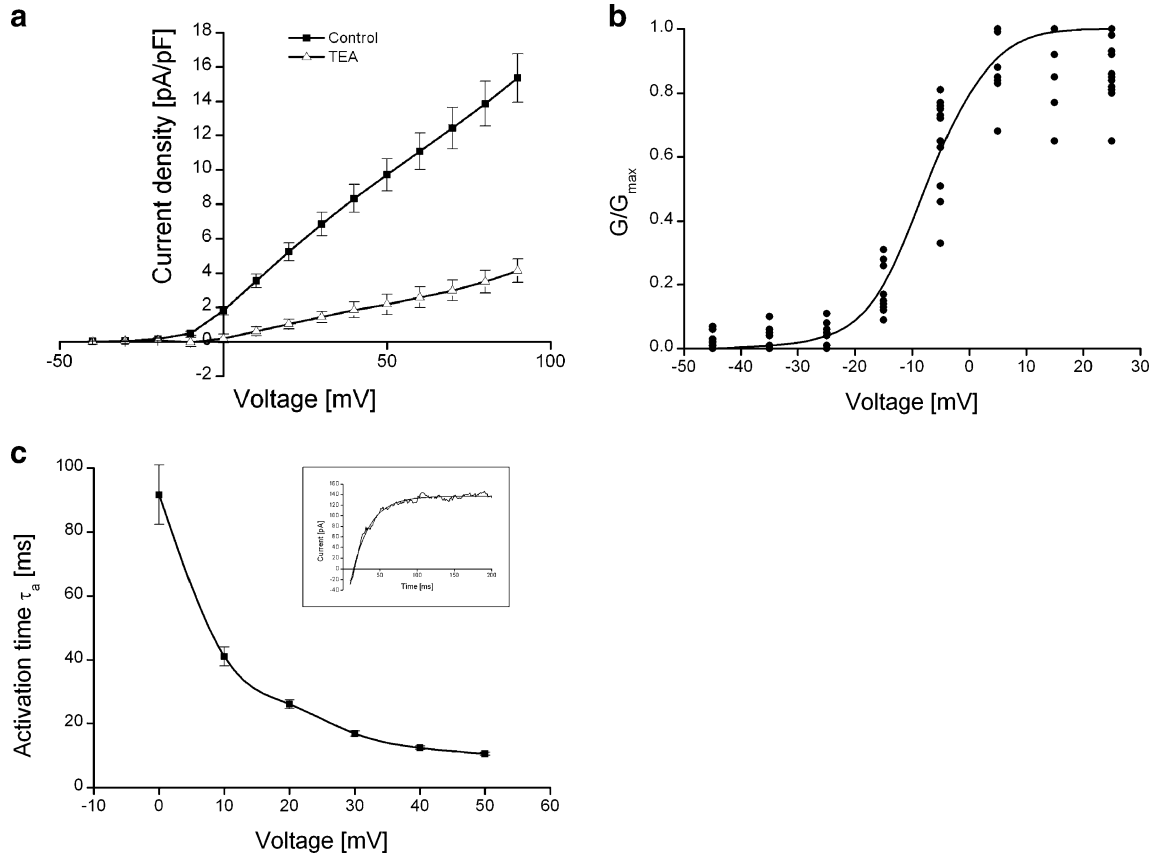

Fig. 5 The pharmacological and electrical properties of the delayed outward current. **a** The currents were activated at depolarization voltages above −30 mV. TEA reduced the current amplitude by more than 70%. DIDS reduced the current by 20–30% (result not shown). The results are averages of 20 cells and eight cells, respectively, for the control experiments and the blockage with TEA. The error bars represent the SEM. **b** The normalized voltage-dependent conductance $G(V)/G_{max}$. The solid line represents a fit of the data points with a simple Boltzmann function. This allowed an estimation of the half-activation voltage, $U_{1/2}$, of −8 mV and an apparent gating charge, z, of 4.8. The results are an average of 11 cells. **c** The activation kinetics of the current was estimated by fitting the time course of the voltage-activated currents (insert) with a single exponential function. The activation time, τ_a, decreased with increasing voltage from a maximal value of 90 ms at 0 mV and reached a minimal value of 13 ms at 50 mV. The results are given as an average and the error bars represent the SEM for 29 cells

voltage-dependent activation of the steady-state current and the kinetics of voltage-dependent activation of the current. The relative steady-state macroscopic conductance-voltage ($G(V)/G_{max}$) curves were determined (Fig. 5b). The $G(V)/G_{max}$ diagrams show that the channels opened at depolarizing voltages above −30 mV. The conductance increased with the voltage to achieve a maximum at 20 mV. The half-maximal voltage of activation ($U_{1/2}$) of −8 mV and the equivalent gating charge (z) of 4.8 were derived by fitting the $G(V)/G_{max}$ curves with a simple Boltzmann distribution.

The activation kinetic was characterized by fitting the currents during the activation time with the single exponential function (Fig. 5c insert) described previously. At very low voltages (−30 mV to 0 mV), the activation was very slow and could not be fit by the exponential equation. This was not due to the depolarization-activated inward current described above because the inhibition of the current with TTX did not affect the activation kinetics of the channels (Fig. 5c). Considering the voltage dependency of the activation, we found that the activation time (τ_a) decreased with the depolarization. A maximal value of 90 ms for τ_a was estimated at 0 mV, and it decreased to reach a minimal value of 13 ms at 50 mV (Fig. 5c).

Discussion

We were able to show, for the first time, that osteoblasts are able to generate repetitive action potentials (Fig. 1). Action potentials in neurons and muscle cells have been correlated with the sequential opening of voltage-gated Na^+ and K^+ channels (Hodgkin and Huxley 1945, 1952). In primary osteoblasts and in the osteoblast-like MG-63 cells, we discovered a membrane potential of approximately −60 mV.

The region between −60 mV and −40 mV was characterized by non-activation of specific currents flanked by two distinguishable regions where voltage pulses activated different currents (Fig. 2). On the left side, the voltage pulses (−150 mV to −60 mV) activated an inward current. On the right side, the voltages pulses between −30 mV and 30 evoked a rapid activated and inactivated inward current and the pulses from −30 mV to 90 mV induced a delayed-activated current (Fig. 2).

The hyperpolarization-activated inward currents

The hyperpolarization between −150 mV and −60 mV induced an inward current characterized by voltage-dependent inactivation (Figs. 2 and 3a). The inactivation could be suppressed by reducing the external Na^+ concentration (results not shown). Inward currents, induced by hyperpolarization of the cell, are due to an influx of cations (K^+) or to an efflux of anions (Cl^-). The observed inward current was registered in the absence of the internal Cl^-, was not affected by DIDS and was completely abolished by an external application of Ba^{2+} (Fig. 3a). Moreover these channels were inactivated by external Na^+ (Data not shown), a characteristic feature of K_{ir} channels (Lee et al. 2007). Additionally, the density of the current increased with increasing $[K^+]_0$, and its reversal potential followed the E_{K^+} from −70 mV to −10 mV at $[K^+]_0$ of 5 mM and 55 mM, respectively (Fig. 3b). These properties indicate that the hyperpolarization-activated inward current was due to the opening of the K_{ir} channels. The current could be measured at an internal pH of 6.5, indicating that it was not related to the pH sensitive channel $K_{ir}1$ or the $K_{ir}4$ subfamily (Dahlmann et al. 2004; Pearson et al. 1999). The current was measured without the activation of G protein-coupled receptors, which suggests that the current does not rely on the G protein-activated $K_{ir}3$ channels (Flagg et al. 2010; Hibino et al. 2010). Finally, the current was measured in the presence of internal ATP, which shows that the ATP-sensitive $K_{ir}6$ channels (Hibino et al. 2010) were not involved. The hyperpolarization-activated inward current was observed at voltages below −60 mV (Figs. 2 and 3), indicating a strong rectification. These results suggest that the current was related to the channels of the $K_{ir}2$ subfamily (Hibino et al. 2010). This conclusion was confirmed by RT-PCR experiments, which show clear mRNA expression of the $K_{ir}2.1$, $K_{ir}2.3$, and $K_{ir}2.4$ channels, the prototypes of the strongly rectifying K_{ir} channels (Fig. 6).

We found that the current was characterized by a half-activation voltage of −73 mV and an apparent gating charge of 2.3. As for the apparent gating charge, it has been shown that in cultivated cells, the inward K^+ channels have a z value between four and six (Hille 2003). Experiments in expression systems, such as *Xenopus* oocytes, estimate the *z* value of the K_{ir} channels to 11–17. These values correspond to the charges of the S4 domain of the channel subunits. The fact that they are not found in the cultivated cells was interpreted as an indication of a reduced population of the channels in the membrane (Hille 2003). This interpretation can be applied to our experiments. We can assume that the MG-63 cells, as well as the primary osteoblasts, express a low density of the $K_{ir}2.x$ channel family. This conclusion is supported by the reduced current density measured, with a maximum of −31 pA/pF (Figs. 2b and 3a).

The depolarization-activated inward current

Depolarization of the cells between −30 mV and 30 mV correlated with a rapid activation followed by an inactivation (Figs. 1 and 4). These are properties of Na_v channels as they have been defined by Hodgkin and Huxley (1952). The measured currents were characterized by a half-activation voltage of −9 mV and by an apparent gating charge of 4.2. These parameters were also found for the Na^+ channels in the giant axon of the crayfish (Hodgkin and Huxley 1952). Therefore, we assume that the depolarization-activated inward current was related to activation of Na_v channels (Fig. 4c). New data from *Xenopus* oocytes show a *z* value of 11–16 for the Na_v channels (Hille 2003). As with the K_{ir} channels, the

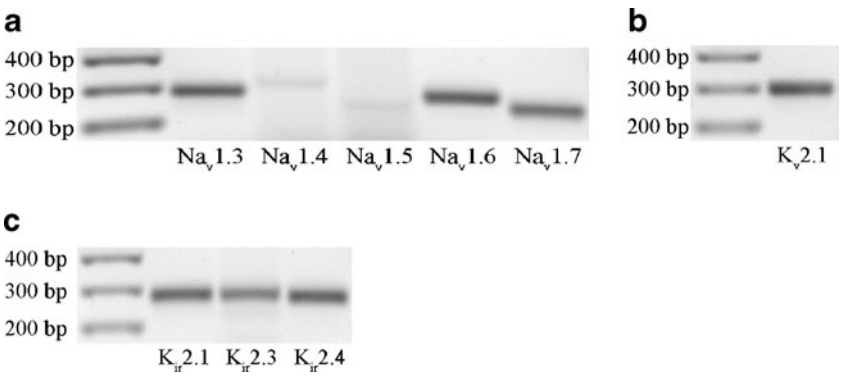

Fig. 6 The channels expressed in the cells as determined by RT-PCR

discrepancy between the values obtained from the original cells and from expression systems has been interpreted as an indication of a reduced channel density in the original cells in comparison to the expression systems (Hille 2003). Therefore, we assume that we have a reduced density of the Na_v channels, which correlated with the observed, reduced maximal current density of −9 pA/pF (Fig. 4a). The conclusion that depolarization opened the Na_v channels is supported by the observation that an increase in internal $[Na^+]$, or by an increase in the external Ca^{2+} concentration, inhibited the current (results not shown). The current was completely suppressed by the application of 50 nM TTX (Fig. 4b), which indicates that the cells are expressing TTX sensitive channels. The pore forming α subunits of the Na_v channels are produced by a gene family with the nine members, named $Na_v1.1$–1.9, which evolved from a single gene by gene duplication (Goldin 2002). The genetic differences correlate to differences in the sensitivity of the channels to TTX. The channels, $Na_v1.1$–1.4, 1.6 and 1.7, are classified as TTX sensitive because they are inhibited by low concentrations of TTX (10–100 nM), while the TTX resistant channels ($Na_v1.5$, 1.8 and 1.9) are inhibited by higher TTX concentrations (10–100 μM) (Goldin 2002; Koopmann et al. 2006; Lei et al. 2004; Narahashi 2008). In our experiments, we found that the depolarization-activated inward current was suppressed by 50 nM TTX (Fig. 4b). We hypothesized that the osteoblasts expressed the TTX sensitive channels, $Na_v1.1$–1.4, 1.6, and 1.7. This hypothesis was verified by RT-PCR experiments, which showed an expression of the TTX sensitive $Na_v1.3$, 1.4, 1.6, and 1.7 channels both in the primary osteoblasts and in the MG-63 osteoblast-like cells (Fig. 6a, b, and c). Additionally, we found mRNA of the TTX-resistant $Na_v1.5$ channel (Fig. 6). However, because we observed that the Na^+ current was completely abolished at very low TTX concentrations, we predict that the mRNA of $Na_v1.5$ is not translated into functional channels. Further, we were not able to determine whether $Na_v1.3$, 1.4, 1.6, and 1.7 equally participate in the formation of the observed channels. Biochemical and cell imaging experiments, beyond the present scope of this paper, should clarify this issue.

The delayed, depolarization-activated outward current

Depolarization above −30 mV gave rise to a delayed-activated outward current, which increased with the increasing depolarization (Figs. 2 and 5a). The Cl^- channel inhibitor, DIDS, reduced the currents by 20–30% and the K^+ channel inhibitor suppressed 70–80% of the current (Fig. 5). These results indicate that the major portion of the outward current was related to the opening of the voltage-activated K^+ channels (K_v). The activation parameters of this current, given by the Boltzmann fitting, had a half-activation of −8 mV and an apparent gating charge of 4.8 (Fig. 5b). The half-activation and the gating charge values indicate that there was a reduced population of K_v channels (Hille 2003). The channels displayed a slow activation, however, an inactivation was not observed (Figs. 2a and 5c insert). At the pharmacological level, the channels were inhibited by TEA (Fig. 5a) and were insensitive to Ba^{2+} and 4-AP (results not shown). The voltage-activated outward K^+ channels are responsible for the membrane repolarization after an action potential. They belong to the family of the six TM K_v channels. This family is divided into four subfamilies, K_v1-4. Each subfamily is characterised by unique activation and inactivation kinetic as well as by a specific pharmacology (Heitzmann and Warth 2008; Nerbonne 2000; Song 2002). The members of the K_v1 and K_v4 subfamilies are characterized by fast activation, a fast inactivation mechanism, and are sensitive to 4-AP. The K_v3 channels activate very fast, have a slow inactivation, and are sensitive to TEA. The K_v2 channels have a slow activation mechanism, are sensitive to TEA, and do not inactivate (Nerbonne 2000). Taken together, this implies that the primary cells, as well as the MG-63 cells, express channels of the K_v2 subfamily. This conclusion was reached because the channels observed displayed slow activation and did not inactivate, and were inhibited by TEA. This assumption is also supported by the voltage-dependent activation kinetic of the channels. We show that the channels have a voltage-dependent activation time (τ_a) with a minimal value of 10 ms, which was achieved at 40 mV (Fig. 5c). A comparable activation time was observed for the $K_v2.1$ channels expressed in *Xenopus* oocytes (Consiglio and Korn 2004). Furthermore, the RT-PCR analysis confirmed the expression of $K_v2.1$ (Fig. 6).

Cellular consequences of the expression of the voltage-activated channels

The concomitant presence of Na_v, K_v, and K_{ir} channels in the neurons, as well as their sequential activation during the depolarization and repolarization process, was postulated as the basis of the action potential (Hodgkin and Huxley 1952). In this report, we observed that MG-63 cells and primary osteoblasts expressed K_{ir}, Na_v and K_v channels, which were sequentially activated upon depolarization. In addition, the cells were able to generate action potentials (Fig. 1). The pharmacology and the electrophysiological parameters of the channels suggests that different types of K_{ir}, Na_v and K_v channels are present, however at a low density compared to excitable cells, such as neurons. We observed that the cells exclusively expressed the slowly activated K_v2 channel subtype. The low channel density and the slow activation of K_v channels are likely respon-

sible for the long duration of the action potential. In the same way, the low density of the Na_v channels could explain the low maximal frequency of the action potential (5 Hz) observed in the cells (Fig. 1). The K_{ir} channels are responsible for setting the resting membrane potential and controlling the excitation threshold. In osteoblasts, we observed the expression of the strongly rectifying $K_{ir}2.1$, $K_{ir}2.3$, and $K_{ir}2.4$ channels. This finding correlates with the polarization (−60 mV). Moreover the strongly rectifying K_{ir} channels and the low density of slow activating K_v channels could explain the non-complete repolarization observed (Fig. 1).

The significance of the action potentials in the osteoblasts is not clear. In excitable cells, the firing of action potentials is a marker of differentiation. We can assume that the presented action potentials and the expressed ion channels in the MG-63 osteoblasts and in the isolated primary osteoblasts could be a characteristic of a developmental state of osteobalst during osteogenesis, which has not been described so far. Moreover, osteoblasts isolated from different persons are variable with respect to the capacity to generate action potentials (result not shown). This may be related to the developmental and pathological state of the isolated cells, for example, whether cells were isolated from healthy or pathogenic (mainly osteoporotic) tissues. Alterations during pathological or developmental changes in bone tissue are mainly analysed on the genetic level (signalling pathways), and the hormonal regulation of the ion channels has not been of great interest as of yet (Zaidi 2007). Evidence has accumulated that ion channels such as melastatin like transient receptor potential 7 (TRPM7), chloride channels, or voltage-operated calcium channels (VOCCs) are involved in development, proliferation and differentiation of osteoblasts (Abed and Moreau 2009; Wang et al. 2010; Zahanich et al. 2005). The present report shows for the first time action potentials and characterizes the expressed voltage dependent channels responsible for the generation the action potentials in the osteoblasts. This report represents therefore a further attempt to characterize the functional physiology of developing osteoblasts.

Acknowledgments The authors thank Prof. Dr. Helge Küster and his team for discussion on the manuscript. The work was supported by the BMBF project NANOTOME (Biophotonik III), the DFG project (Transregio 37) and by Boehringer Ingelheim International GmbH.

References

Abed E, Moreau R (2009) Importance of melastatin-like transient receptor potential 7 and magnesium in the stimulation of osteoblast proliferation and migration by platelet-derived growth factor. Am J Physiol Cell Physiol 297:C360–C368

Bezanilla F (2007) Voltage-gated ion channels. In: Chung SH, Andersen OS, Krishnamurthy V (eds) Biological membrane ion channels: dynamics, structure and applications. Springer Science + Business Media, LLC, pp 81–118

Bichet D, Haass FA, Jan LY (2003) Merging functional studies with structures of inward-rectifier K^+ channels. Nat Rev Neurosci 4:957–967

Bosmans F, Tytgat J (2007) Voltage-gated sodium channel modulation by scorpion α-toxins. Toxicon 49:142–158

Catterall WA, Goldin AL, Waxman SG (2003) International union of pharmacology. XXXIX. Compendium of voltage-gated ion channels: sodium channels. Physiol Rev 55:575–578

Clay JR (2005) Axonal excitability revisited. Prog Biophys Mol Biol 88:59–90

Consiglio JF, Korn SJ (2004) Influence of permeant ions on voltage sensor function in $K_V2.1$ potassium channel. J Gen Physiol 123:387–400

Dahlmann A, Li M, Gao ZH, McGarrigle D, Sackin H, Palmer LG (2004) Regulation of K_{ir} channels by intracellular pH and extracellular K^+: mechanism of coupling. J Gen Physiol 123:441–454

de Boer TP, Houtman MJC, Compier M, van der Heyden MAG (2010) The mammalian $K_{ir}2.x$ inward rectifier ion channel family: expression pattern and pathophysiology. Acta Physiol 199:243–255

Flagg TP, Enkvetchakul D, Koster JC, Nichols CG (2010) Muscle K_{ATP} channels: recent insights to energy sensing and myoprotection. Physiol Rev 90:799–829

Fozzard HA, Lipkind GM (2010) The tetrodotoxin binding site is within the outer vestibule of the sodium channel. Mar Drugs 8:219–234

Gallagher JA (2003) Human osteoblast culture. Meth Mol Med 80:3–18

Goldin AL (2002) Evolution of voltage-gated Na^+ channels. J Exp Biol 205:575–584

Hanck DA, Fozzard HA (2007) Voltage-gated sodium channels. In: Chung SH, Andersen OS, Krishnamurthy V (eds) Biological membrane ion channels: dynamics, structure and applications. Springer Science + Business Media, LLC, pp 219–239

Heitzmann D, Warth R (2008) Physiology and pathophysiology of potassium channels in gastrointestinal epithelia. Physiol Rev 88:1119–1182

Hibino H, Inanobe A, Furutani K, Murakami S, Findlay I, Kurachi Y (2010) Inwardly rectifying potassium channels: their structure, function, and physiological roles. Physiol Rev 90:291–366

Hille B (2003) Ion channels of excitable membranes, 3rd edn. Sinauer Associates Press, Sanderland

Hodgkin AL, Huxley AF (1945) Resting and action potentials in single nerve fibres. J Physiol 104:176–195

Hodgkin AL, Huxley AF (1952) A quantitative description of membrane current and its application to induction and excitation in nerve. J Physiol 117:500–544

Koopmann TT, Bezzina CR, Wilde AAM (2006) Voltage-gated sodium channels: action players with many faces. Ann Med 38:472–482

Korn SJ, Trapani JG (2007) Voltage-gated potassium channels. In: Chung SH, Andersen OS, Krishnamurthy V (eds) Biological membrane ion channels: dynamics, structure and applications. Springer Science + Business Media, LLC, pp 119–170

Lee CH, Ruben PC (2008) Interaction between voltage-gated sodium channels and the neurotoxin, tetrodotoxin. Channels 2:407–412

Lee DH, Kimm K, Kim HL, Han BG (2007) Heterogeneous composition of voltage-dependent K^+ currents in hepatic stellate cells. Yonsei Med J 48:684–693

Lei M, Jones SA, Liu J, Lancaster MK, Fung SSM, Dobrzynski H, Camelliti P, Maier SKG, Noble D, Boyett MR (2004) Require-

ment of neuronal- and cardiac-type sodium channels for murine sinoatrial node pacemaking. J Physiol 559:835–848

Lipkind GM, Fozzard HA (1994) A structural model of the tetrodotoxin and saxitoxin binding site of the Na^+ channel. Biophys J 66:1–13

Narahashi T (2008) Tetrodotoxin: a brief history. Proc Jpn Acad Ser B Phys Biol Sci 84:147–154

Nerbonne JM (2000) Molecular basis of functional voltage-gated K^+ channel diversity in the mammalian myocardium. J Physiol 525:285–298

Oliver D, Baukrowitz T, Fakler B (2000) Polyamines as gating of inward rectifier K^+ channels. Eur J Biochem 267:5824–5829

Olsen ML, Sontheimer H (2008) Functional implications for $K_{ir}4.1$ channels in glial biology: from K^+ buffering to cell differentiation. J Neurochem 107:589–601

Panama BK, Lopatin AN (2006) Differential polyamine sensitivity in inwardly rectifying $K_{ir}2$ potassium channels. J Physiol 571:287–302

Pearson WL, Dourado M, Schreiber M, Salkof L, Nichols CG (1999) Expression of a functional $K_{ir}4$ family inward rectifier K^+ channel from a gene cloned from mouse liver. J Physiol 514:639–653

Penzotti JL, Lipkind G, Fozzard HA, Dudley SC Jr (2001) Specific neosaxitoxin interactions with the Na^+ channel outer vestibule determined by mutant cycle analysis. Biophys J 80:698–706

Ruppersberg JP (2000) Intracellular regulation of inward rectifier K^+ channels. Pflügers Arch Eur J Physiol 441:1–11

Song WJ (2002) Genes responsible for native depolarization-activated K^+ currents. Neurosci Res 42:7–14

Wang H, Mao Y, Zhang B, Wang T, Li F, Fu S, Xue Y, Yang T, Wen X, Ding Y, Duan X (2010) Chloride channel ClC-3 promotion of osteogenic differentiation through Runx2. J Cell Biochem 111:49–58

Zahanich I, Graf EM, Heubach JF, Hempel U, Boxberger S, Ravens U (2005) Molecular and functional expression of voltage-operated calcium channels during osteogenic differentiation of human mesenchymal stem cells. J Bone Miner Res 20:1637–1646

Zaidi M (2007) Skeletal remodeling in health and disease. Nat Med 13 (7):791–801